LEGIBILITY NOTICE

A major purpose of the Technical Information Center is to provide the broadest dissemination possible of information contained in DOE's Research and Development Reports to business, industry, the academic community, and federal, state and local governments.

Although a small portion of this report is not reproducible, it is being made available to expedite the availability of information on the research discussed herein.

LA-UR - 90-496

CONF-900300--1

MAR 0 5 1990

Los Alamos National Laboratory is operated by the University of California for the United States Department of Energy under contract W-7405-ENG-36

LA-UR--90-496

DE90 007536

TITLE: Laser-Matter Interaction at Intensities of 10^{12} Watt/Cm^2 and Below

AUTHOR(S) S. R. Goldman, R. S. Dingus, R. C. Kirkpatrick, R. A. Kopp, E. K. Stover, and R. G. Watt

SUBMITTED TO International Congress on Optical Science and Engineering, March 12-16, 1990, The Hague, The Netherlands

DISCLAIMER

MASTER

Los Alamos Los Alamos National Laboratory
Los Alamos, New Mexico 87545

Laser-matter interaction at intensities of 10^{12} W/cm^2 and below

S. Robert Goldman, Ronald S. Dingus, Ronald C. Kirkpatrick, Roger A. Kopp,
Elmer K. Stover, and Robert G. Watt

Los Alamos National Laboratory
Los Alamos, NM 87545, USA

ABSTRACT

For single pulsed laser-matter interactions at sufficiently high intensity, the electron density in the ablated vapor is large enough to absorb the laser radiation before it can reach the dense target material. The resulting interaction can be described in terms of energy flows: laser energy is absorbed in the plasma in front of the target and reappears as thermal electron energy and secondary radiation, part of which impinges upon and heats the dense target material at the dense material-vapor interface. This heating in turn drives ablation, thereby providing a self-consistent mass source for the laser absorption, energy conversion, and transmission Under typical conditions of laser intensity, pulse width and spot size, the flow patterns can be strongly two-dimensional. We have modified the inertial confinement fusion code LASNEX to simulate gaseous and some dense material aspects for the relatively low intensity, long pulse-length conditions of interest in many laser-related applications. The unique aspect of our treatment consists of an ablation model which defines a dense material-vapor interface and then calculates the mass flow across this interface. The model, at present, treats the dense material as a rigid, two-dimensional simulational mass and heat reservoir, suppressing all hydrodynamical motion in the dense material. The modeling is being developed and refined through simulation of experiments, as well as through the investigation of internal inconsistencies, and some simulation of model problems. The computer simulations and additional post-processors provide a wealth of predictions for possible measurements, including impulse given to the target, pressures at the target interface, electron temperatures and densities, and ion densities in the vapor-plasma plume region, transmission and emission of radiation along chords through the plume, total mass ablation from the target and burn-through of the target material at selected radial locations. We will present an analysis of some relatively well-diagnosed experimental behavior which has been useful in development of our modeling.

1. INTRODUCTION

Within this paper we consider a modeling technique and its application to the calculation of laser-matter interaction scenarios for laser intensities I, pulse-widths τ, wavelengths λ, and energies E with: $10^6 \leq I \leq 10^{12}$ W/cm^2, $10^{-8} \leq \tau \leq 10^{-4}$ sec, $0.25\mu m \leq \lambda \leq 10.6$ μm, $E \leq 5 \times 10^3$ J. For simplicity we have treated only flat aluminum targets with low background densities of order 10^{-8} g/cm^3. For this parameter range the laser energy need not couple directly into the dense target material, but rather it can be absorbed by the vapor which has ablated from the target and formed a plasma. Hence the interaction is strongly non-linear in terms of either the laser fluence or intensity. At conditions well above the threshold for plasma formation, the laser-matter interaction tends to be material independent[1], and the material properties of aluminum are relatively well characterized. This has enabled us to concentrate on hydrodynamic and energy transport behavior in the plasma outside the target rather than on material properties.

Comparison of two-dimensional simulations with the impulse delivered to a target has suggested the significance of two-dimensional effects.[1,2] From standard rough estimates, problems in this parameter range can readily be two-dimensional even for laser beams with direction of propagation normal to the target. Analytically, two-dimensionality of the vapor behavior is estimated through the parameter $\hat{\tau} = c_s \tau / d$, where c_s is a typical sound speed in the aluminum vapor, and d is the laser spot size; problems with $\hat{\tau} \geq 1$ are expected to be significantly two-dimensional. For the laser conditions which we will analyze in some detail below, from a run with the KMS Chroma laser[3], $E = 2 \times 10^3$ J, $d = 0.8$ cm, $\tau = 10^{-5}$ sec, and $\hat{\tau} \approx 10$.

In Section 2., we discuss details of our simulational modeling with emphasis on the treatment of ablation behavior. In Section 3., using the results from simulation of the KMS shot alluded to above, we present a picture of the energy and hydrodynamic flows obtained through the simulations. In Section 4., we compare our simulational

results against the shot. In Section 5., we assess the adequacy of the modeling and directions for further modeling and experimental effort.

2. MODELING (WITH EMPHASIS ON ABLATION)

We have modified the inertial fusion code LASNEX to simulate gaseous and some dense material aspects of the relatively low intensity, long pulse-length conditions within the parameter range of interest. We use a two-dimensional r,z grid with a finite difference zonal representation for both the gaseous and the dense material regions. The unique aspect of the modeling within the context of LASNEX consists of an ablation model which defines the dense material-vapor interface on the basis of density, and then calculates the mass flow across this interface. The model, at present, suppresses hydrodynamics in the dense region, so that in effect it is a rigid, two-dimensional heat reservoir. The penalty is a loss of physical reality; the gain is the tractability of the problem.

Typically, in the past, in two-dimensional calculations, when we tried to combine solid dynamics with gaseous behavior for the time scales of interest, the time steps due to the solid behavior were so small and the solid behavior so erratic as to make the calculations prohibitively lengthy and obviously unreliable. It did not appear possible to use a single phase equation of state to describe the liquid-vapor transition for aluminum, probably because, with p denoting pressure, and ρ denoting density, the hydrodynamics is unstable when $\partial p/\partial \rho < 0$. For a two phase equation of state, with Maxwell construction, $\partial p/\partial \rho$ is discontinuous at the upper density end, especially, and also the lower density end of the phase transition. With explicit hydro calculations, very small increases in density resulted in large incorrect pressure jumps.

For the ablation model, in similarity to the treatment of drop evaporation in Zel'dovich and Raizer[4], one considers jump conditions across a dense material-vapor interface. Let:

p_{cc} = Clausius-Clapeyron dense material vapor pressure,
p = pressure of the gas in the first zone outside the dense material interface,
ρ = density of the gas in the first zone outside the dense material interface,
v = effective velocity of ablated gas at the interface.

For an abrupt transition between dense material and vapor, i.e. such that the transition region has negligible mass, momentum and energy, one has:

$$p_{cc} = p + \rho v^2, \tag{1}$$

from which, for μ the mass ablation rate per unit area:

$$\mu = \rho v = \left((p_{cc} - p)\rho\right)^{1/2}. \tag{2}$$

In the limit of a vacuum outside the target, for which p and $\rho \rightarrow 0$, one anticipates that the density of the ablated material should be the saturated vapor density, ρ_{sat}, at the target surface temperature. To account for this situation we use:

$$\mu = \left((p_{cc} - p)\rho^*\right)^{1/2}, \tag{3}$$

with ρ^* the maximum of ρ_{sat} and ρ.

Over a time step, the mass ablation rate results in a recession of the dense material boundary. This is accomplished through a rezoning step in which the mesh points along the interface are displaced to accommodate for the loss of ablated material. Less frequently the mesh points in the dense region are rezoned so that the zones there do not "bowtie" due to the motion of the interface.

The energy flux corresponding to the mass flux μ is taken to be μL_v^*, where L_v^* is the lesser of L_v, the latent heat of vaporization, and $(\epsilon_v - \epsilon_d)$, where ϵ_v is the specific internal energy of the vapor material, and ϵ_d is the specific internal energy of the dense material. L_v is assumed to be constant. By taking L_v^* in place of L_v, we allow for representation of the phase transition to some extent since the material need not have as a large a specific internal energy as fully vaporized material. Energy is transported conservatively across the interface when it is rezoned.

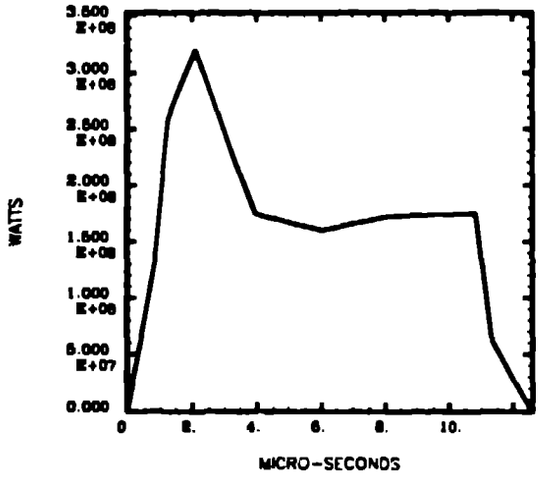

Figure (1) Laser power profile for the analyzed shot.

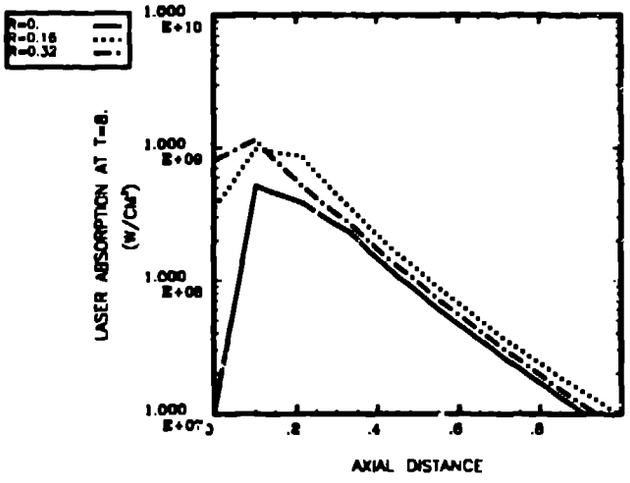

Figure (2) Profiles of laser energy deposition in the vapor.

The force per unit area exerted on the solid by the vapor is given by $p + \rho v^2$. The momentum imparted to the dense material is calculated from the time and area integral of this term. Since the interface is not allowed to acquire velocity (other than through the ablative recession), the force exerted on the vapor at the interface is the same in magnitude and opposite in direction.

Other elements of the modeling include:

1. Both vapor and dense regions are treated in LTE.
2. Radiation is treated through multi-group diffusion using the Los Alamos LEDCOP (Light Element Detailed Configuration Opacity) tables, typically defined over electron temperatures from 0.25 eV to 150 eV.
3. Correspondingly, there are the order of 35 photon groups defined over photon energies from 0.01 eV to 150 eV.
4. The laser deposition is done by a ray trace package which propagates the laser rays in three dimensions through the cylindrically symmetric (r,z) mesh. The ray prescription is chosen to conform the particular optics of the problem; in general the intensity is not uniform within the laser spot, and the rays make non-zero angles with the z-axis.
5. All photon groups *including the laser photon group* have an absorption and emission with bound-bound, bound-free, and free-free contributions.
6. The gaseous vapor region is represented by a two-dimensional (r,z) Lagrangean mesh with extensive rezoning.

3. SIMULATIONAL DESCRIPTION OF THE LASER-MATTER INTERACTION

In this section, we present some of the results from the computer simulation of the shot whose gross parameters are noted in the introduction. Although, as will be clear from comparison with the experimental data, the agreement with experiment is not complete, the mechanisms treated in the simulation, and the type of outputs possible, are suggestive of necessary modeling elements and directions for further measurement and theoretical treatment.

The Chroma laser emits at 1.06 μm. The fluence was of the order of 4×10^3 J/cm^2, and the mean intensity was of the order of 4×10^8 W/cm^2. The experimental laser pulse profile is indicated in Figure 1.

The simulations indicate a scenario in which the target material in the laser spot is rapidly heated through the melt temperature and the atmospheric boiling temperature, producing a plasma which tends to shield the target from much of the subsequent direct laser radiation. The resulting interaction can be described in terms of energy flows: most of the laser energy is absorbed in the plasma in front of the target and reappears as thermal electron energy and secondary radiation, part of which, together with the penetrating laser radiation, impinges upon and

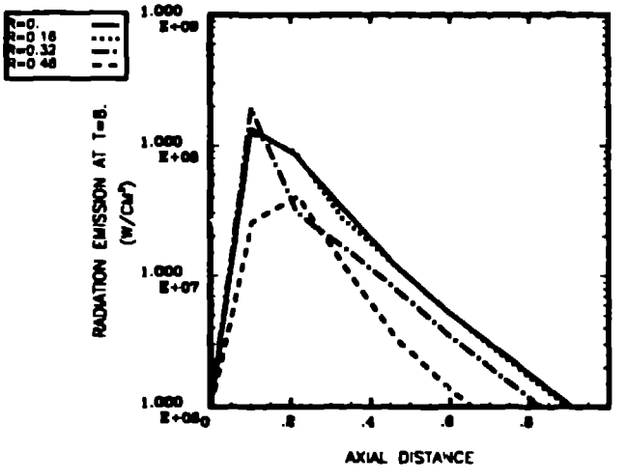

Figure (3) Profiles of re-radiation emission in the vapor.

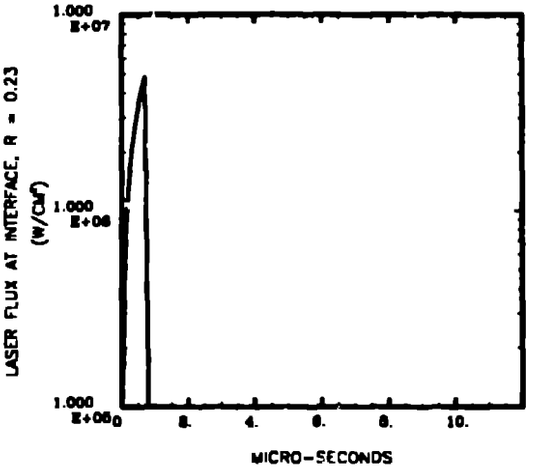

Figure (4) Time profile of the laser flux incident on the target interface at r = 0.23 cm.

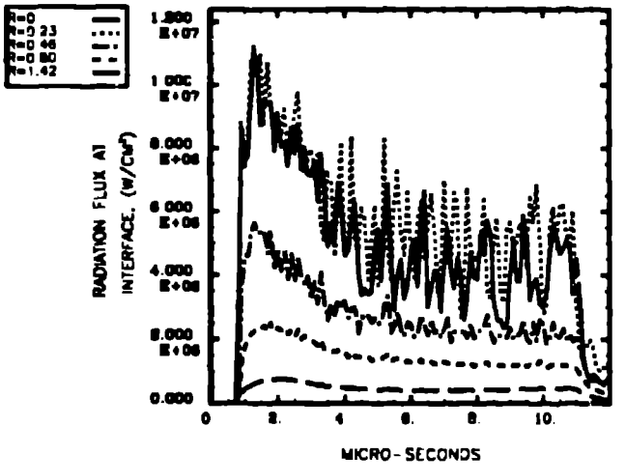

Figure (5) Re-radiation flux on the target interface.

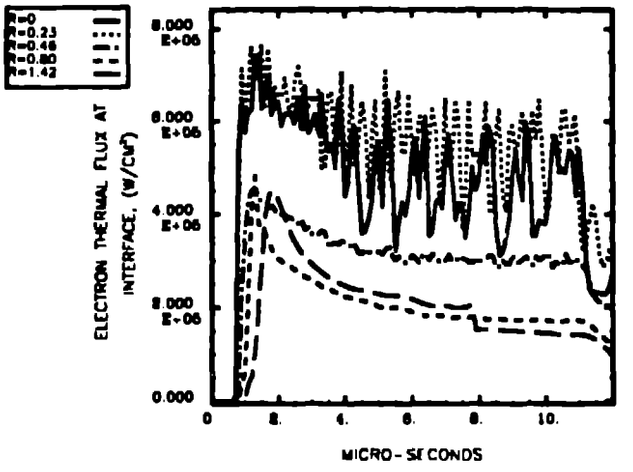

Figure (6) Electron thermal flux on the target interface.

heats the dense target material at the dense material-vapor interface. This heating in turn drives ablation, thereby providing a self-consistent mass source for the laser absorption, energy conversion, and transmission.

Volume deposition of the laser flux and the subsequent re-emission of radiation are indicated in Figures 2 and 3. The laser flux, re-radiation flux, and thermal electron flux at the interface are shown respectively in Figures 4-6. It is clear that radiation flux is the dominant energy transport mechanism to the dense material once the plasma has been established in the vapor region, especially when one considers that only a small fraction of the incident laser light is likely to be absorbed by the dense material. The mass ablation rate at a particular location and the total ablated mass as a function of location along the interface and time are shown in Figures 7 and 8, respectively. The fluctuations in the mass ablation rate are attibutable to fluctuations in the pressure as shown in Figure 9. The increased mass ablation near the outside of the laser spot, but within it, is due to the lowering of density within increasing radius due to radial mass flow due to the pressure gradient at the edge of the laser spot.

Further information on the plasma variables for the vapor region is provided by Figures 10-12 which present respectively the electron density, the mass density and the electron temperature for an extended volume in the

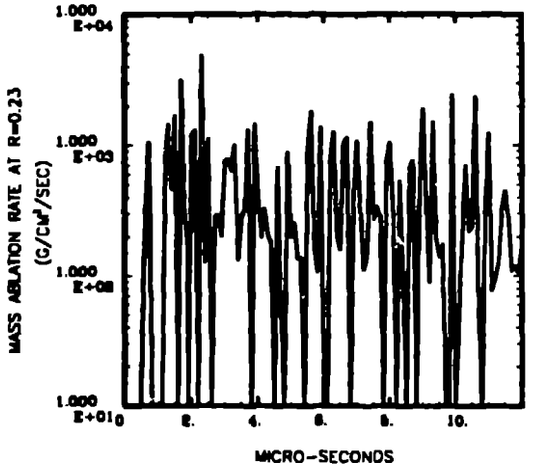

Figure (7) The mass ablation rate at a radius of r=0.23.

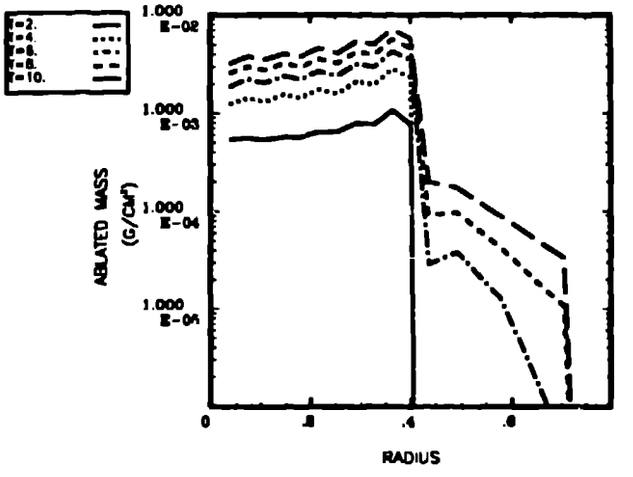

Figure (8) Ablated mass along the interface. The laser spot diameter is 0.8 cm.

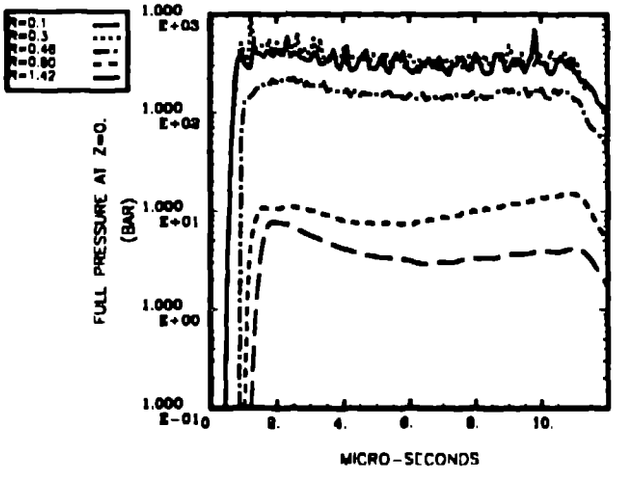

Figure (9) Total pressure at the target interface [static pressure (p) + ram pressure (ρv^2).]

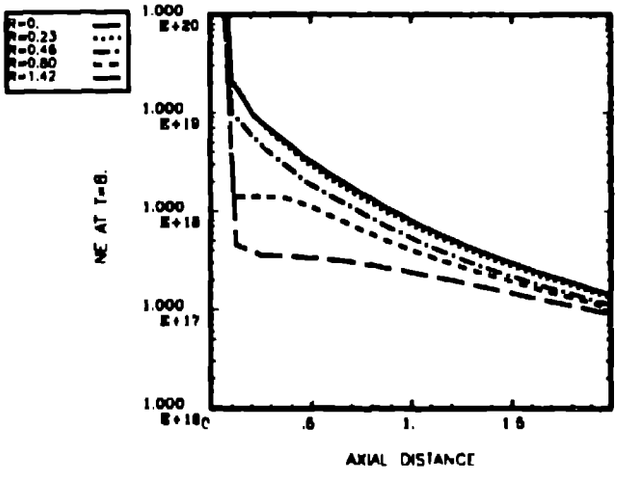

Figure (10) Electron density (cm^{-3}) in the vapor at $t = 8\mu$sec. (Values at axial distances $\leq$ 0.1cm. should be disregarded.)

vapor at a time of 8 μsec into the laser pulse. It is interesting to note that although the laser deposition as shown in Figure 2 varies with radius within the laser spot, there is almost no variation indicated for these variables, indicating the role of energy transport in smoothing out profiles in density and temperature. The gradients are largest closest to the target, with some suggestion of sizes smaller than the laser spot size. Such behavior is not unreasonable when one considers that thermal transport can impose length scales on a problem additional to those due to the hydrodynamic flow expansion.

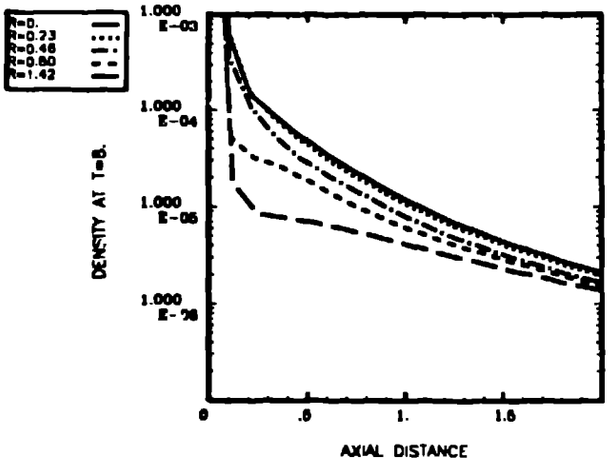

Figure (11) Mass density (gm/cm^{-3}) in the vapor at $t = 8\mu$sec. (Values at axial distances $\leq$ 0.1cm. should be disregarded.)

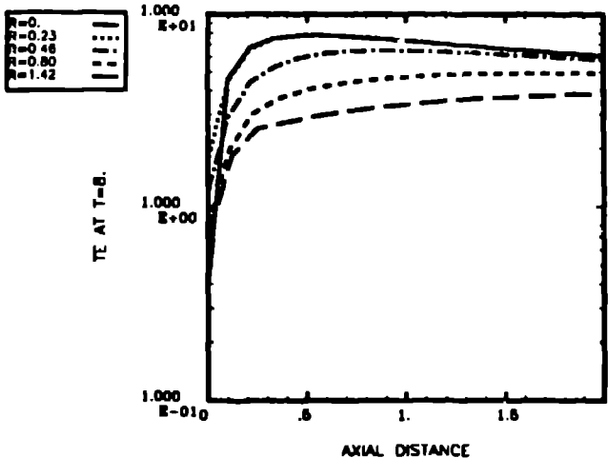

Figure (12) Electron temperature (eV) in the vapor at $t = 8\mu$sec. (Values at axial distances $\leq$ 0.1cm. should be disregarded.)

4. COMPARISON OF SIMULATIONAL RESULTS WITH EXPERIMENTAL DATA

A number of points of comparison between experiment and simulation are shown in Table I:

TABLE I. COMPARISON OF EXPERIMENT AND SIMULATION

	EXPERIMENT	SIMULATION
Momentum coupling efficiency (dyne-sec/Joule)	0.8-1.3	1.35
Peak pressure on target (bar)	400-700	700-1000
(Impulse "outside" laser spot)/(impulse "inside" laser spot)	1:1	3:7
Burn diameter on target (cm)	2.6	4.0
Total ablated mass (mg)	0.9	0.4

The momentum coupling efficiency is defined as the ratio of impulse imparted to the target to incident laser energy. The range for simulational peak pressure is gotten by either neglecting or including the two highest pressure spikes shown in Figure 9. Impulse "outside" the laser spot includes all impulse imparted to the target from the pressure at locations of radius greater than 0.5 cm, and "impulse" inside the laser spot is the remaining impulse imparted to the target. The experimental burn diameter is the diameter of the region within which the aluminum surface texture is strongly modified. In the calculations this location is identified by the outer radius of target surface temperatures above the melt temperature ($\approx$ 0.08eV.)

Additional experimental data[5] for emission and transmission at 515 nm for chords passing 0.1 cm in radius off the target symmetry axis at various axial locations off the target are shown in Figures 13 and 14.

The simulational results can be categorized against the experimental results in the following manner:

1. The impulse within the laser spot is greater in the simulations.
2. The impulse is more centralized to the laser spot in the simulations.
3. Radiation emission from the laser spot is greater in the simulations.
4. The difference in mass loss undoubtedly involves the exclusion of melt-splash processes in the simulations.
5. The optical thickness of the plume is less in the simulations than in the experiments. This can be seen directly from Figure 14, or indirectly by combining the results of Figures 3, 4, and 13 (e.g. Figures 3 and 4 indicate that the laser absorption and re-radiation emission regions overlap strongly, and Figure 13 indicates that

the experimental re-radiation occurs further off the target than the calculated reemission.) Hence it is plausible that the incident laser radiation is absorbed further off the target than in the simulations.

6. Results for full ablation are closer to experimental transmission and absorption than those for diminished ablation.

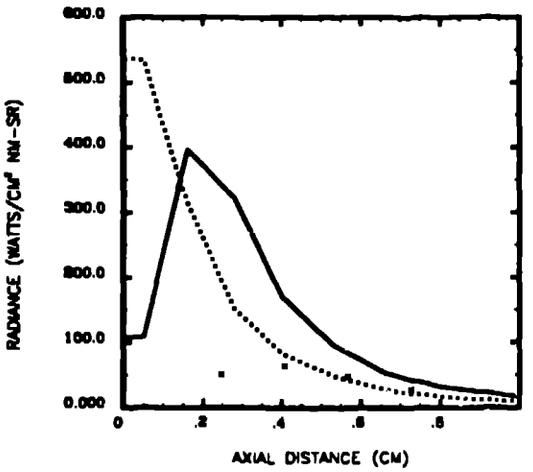

Figure (13) Emission at 515 nm for chords passing 0.1 cm in radius off the symmetry axis as a function of axial location at t=4.8 μsec. The solid line denotes calculations with full mass ablation; the dashed line denotes results with the mass ablation artificially decreased to about one half of its expected value; the points are obtained from measurement[5].

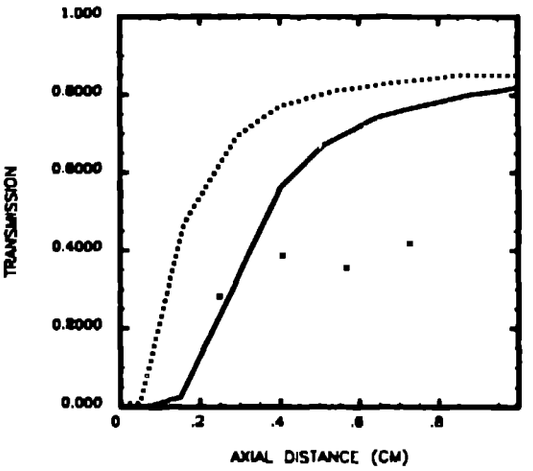

Figure (14) Transmission at 515 nm for chords passing 0.1 cm in radius off the symmetry axis as a function of axial location at t=4.8 μsec. Notation the same as for preceding figure.

5. ADEQUACY OF MODELING AND EXTENSIONS

In general it is clear at this point that the experimental data is fragmentary, and that there is a need even for repeated measurements of the quantities which have already been measured. Determination of the following variables would be useful in evaluating and extending any simulational results:

1. pressure on target as a function of position and time,
2. target emission and transmission in the near UV as well as for optical wavelengths,
3. spatial and temporal profiles of electron density and temperature,
4. multi-group opacities.

Theoretically one must pay continued attention to the numerical accuracy of the algorithms (for instance, in rezoning) and their suitability to the problem. (As an example: Is radiation diffusion appropriate for the radiation energy transport?)

Perhaps the most interesting theoretical extension of the results lies in the consideration of liquid effects. Liquid elements could be found in the vapor volume either through melt-splash sources or through the recondensation of vapor at cooler temperatures outside the target plume[4,5].

The difference between experimental mass loss and calculated mass loss could readily be attributed to melt-splash behavior. What is unclear is whether the presence of splashed droplets in the vapor region could have a significant effect on the vapor behavior. From direct examination of targets, atleast a portion of melt splash flow is predominantly radial along the target rather than axially outwards. Also, droplets moving off the target surface

and present at locations of say, several mm, away from the surface before the end of the laser pulse, would have to move at velocities of order 10^5 cm/sec.

Nevertheless, the presence of droplets from the target in the laser plume could reconcile some of the differences between theory and experiment. From Figures 13 and 14, the agreement of theory with experiment would be improved by an increased amount of mass ablation in the simulations. The ablated material would be cooler and denser so that transmission would be lower, laser energy would be absorbed further off target and emission would be lower. The difficulty with this picture is that the aluminum surface is apparently ablated through the deposition of re-radiated energy. With greater mass loss, the re-reradiation in the simulations is decreased but the requirement on radiation to sustain the increased ablation is increased. The problem could be resolved if material left the ablation surface as liquid and then moved off the target into the vapor region before being fully ablated *or indeed, by any other mechanism which would increase ablation without increasing the demand for energy flux through the ablation surface.*

The presence of recondensed droplets in the cooler region around the plume offers an alternate means of reducing emission and transmission to bring the theoretical results more in line with experiment. The consideration of this mechanism would appear to require less modification of the modeling because the affected region is outside the plume, within which the dynamics affecting coupling to the target is most non-linear. A quantitative treatment is currently lacking.

Finally, we note that the field of laser interaction with targets at moderate intensities is a rich mixture of many different physical effects and areas of interest, and that we are only beginning to explore it in a detailed manner. The simulational work which we have done provides a useful framework for investigation of this area. We anticipate with continued simulational development and cross-comparison with experiment that we will obtain an improved understanding of the necessary scientific components. It is our expectation that such study will be fruitful from the standpoints of both pure and applied science.

6. ACKNOWLEDGMENTS

It is a pleasure to thank David Rosen for helpful discussions of his experimental data and its interpretation. This work was supported in part by the United States Department of Energy and in part by DNA.

7. REFERENCES

1. R. S. Dingus and S. R. Goldman, "Plasma Energy Balance Model for Optical-Laser-Induced Impulse in Vacuo," *Proceedings of the International Conferences on Lasers '86*, pp. 111-122, Orlando, Florida, 1986.

2. S. R. Goldman, S. L. Gitomer, R. A. Kopp, J. S. Saltzman and R. S. Dingus, "Simulation of Laser-Target Interactions in a Vacuum," *Proceedings of the AIAA Laser Effects and Target Response Meeting*, Menlo Park, CA, November, 1985, *Los Alamos National Laboratory Document*, LA-UR 85-4047.

3. R. G. Watt, R. S. Dingus, S. R. Goldman, R. E. L. Green, R. Kopp, J. Kephart, L. Lee and T. J. Roemer, "Long Pulse-Length Laser-Target Interactions at 1 μm: Recent Experiments and Analysis," *Los Alamos National Laboratory Document*, LA-UR 88-1144.

4. Y. B. Zeldovich and Y. P. Raizer, *Physics of Shock Waves and High-Temperature Hydrodynamic Phenomena*, vol 2, Chapter 8, Academic Press, New York, 1966.

5. D. Rosen, I. Arvin, and C. Rollins, "Plasma Self-Transmission Measurements in Support of Long-Pulse Impulse Coupling Test Series," *PSI-1021/TR-647*, Physical Sciences Inc., Andover MA, February, 1987.